

RE-MCDF: Closed-Loop Multi-Expert LLM Reasoning for Knowledge-Grounded Clinical Diagnosis

Shaowei Shen[†], Xiaohong Yang[†], Jie Yang, Lianfen Huang^{*},
Yongcai Zhang, Yang Zou, Seyyedali Hosseinalipour

Abstract—Electronic medical records (EMRs), particularly in neurology, are inherently heterogeneous, sparse, and noisy, which poses significant challenges for large language models (LLMs) in clinical diagnosis. In such settings, single-agent systems are vulnerable to self-reinforcing errors, as their predictions lack independent validation and can drift toward spurious conclusions. Although recent multi-agent frameworks attempt to mitigate this issue through collaborative reasoning, their interactions are often shallow and loosely structured, failing to reflect the rigorous, evidence-driven processes used by clinical experts. More fundamentally, existing approaches largely ignore the rich logical dependencies among diseases, such as mutual exclusivity, pathological compatibility, and diagnostic confusion. This limitation prevents them from ruling out clinically implausible hypotheses, even when sufficient evidence is available. To overcome these, we propose RE-MCDF, a relation-enhanced multi-expert clinical diagnosis framework. RE-MCDF introduces a *generation-verification-revision closed-loop* architecture that integrates three complementary components: (i) a primary expert that generates candidate diagnoses and supporting evidence, (ii) a laboratory expert that dynamically prioritizes heterogeneous clinical indicators, and (iii) a multi-relation awareness and evaluation expert group that explicitly enforces inter-disease logical constraints. Guided by a medical knowledge graph (MKG), the first two experts adaptively reweight EMR evidence, while the expert group validates and corrects candidate diagnoses to ensure logical consistency. Extensive experiments on the neurology subset of CEMR (NEEMRs) and on our curated dataset (XMEMRs) demonstrate that RE-MCDF consistently outperforms state-of-the-art baselines in complex diagnostic scenarios.

Index Terms—Clinical Diagnosis, Knowledge Graph, Large Language Models, Smart Healthcare.

I. INTRODUCTION

The proliferation of large language models (LLMs) has demonstrated immense potential in clinical narrative understanding and generation, particularly for diagnosing cerebrovascular diseases in neurology [1], [2]. Typically, these models derive diagnostic conclusions by synthesizing multi-source evidence from electronic medical records (EMRs). However, LLMs often lack the complex, multi-step reasoning capabilities required to synthesize heterogeneous and noisy clinical evidence into rigorous diagnoses. Moreover, LLM-driven diagnostic reasoning remains susceptible to hallucinated inferences, incomplete medical coverage, and poorly calibrated confidence, which can lead to unreliable clinical decisions [3].

To address these, contemporary research has largely followed two major paradigms for improving LLM-based clinical diagnosis: (i) *Prompt-based reasoning strategies*, such as chain-of-thought (CoT), tree of thoughts (ToT), and self-consistency, which aim to bolster reasoning quality and output stability [4]–[6]. However, these reasoning chains are typically expressed in natural language; while they offer some improvement in reliability, they defy systematic verification. Furthermore, in complex scenarios with lengthy records or comorbidities, models remain susceptible to distraction by irrelevant cues, resulting in unreliable candidate generalization and interpretability [7], [8]. (ii) *The integration of knowledge graph (KG) as a structured medical knowledge substrate*, which creates a synergistic LLM-KG paradigm designed to mitigate LLM deficiencies regarding factual coverage and verifiability [9]–[11]. Within this paradigm, prior work generally follows one of two architectural strategies. (A) *Loosely-Coupled Parallel Fusion* ($LLM \oplus KG$), where the LLM generates candidates or extracts key entities while a parallel process executes retrieval and re-ranking on the KG, with the results from these dual pathways subsequently aggregated at the final stage [12], [13]. (B) *Deep Collaborative Reasoning* ($LLM \otimes KG$), which embeds the LLM directly into the graph reasoning process, and entails iterative expansion, node selection, and evidence aggregation for constructing structured reasoning trajectories over the graph [14], [15]. Beyond such single-agent designs, recent diagnostic systems increasingly explore the synergy between multi-agent collaboration and graph-based reasoning, which has shown promise in handling complex medical decision-making scenarios [16]–[18].

Despite the advancements achieved by the above methods in general tasks, their direct adaptation to the *diagnosis of cerebrovascular diseases in neurology based on EMRs* remains confronted with three fundamental challenges. **Challenge 1: Static evidence weighting under heterogeneity.** Existing models often adopt a binary *existence-as-match* paradigm for KG evidence, lacking the expert-like ability to dynamically assess the relative importance of heterogeneous and abnormal clinical indicators. As a result, fine-grained evidence prioritization is not achieved. **Challenge 2: Neglect of inter-disease logical constraints.** Most frameworks (single/multi agent) focus on accumulating isolated evidence rather than modeling complex logical relationships (e.g., mutual exclusion and differential

[†] Equal Contribution, ^{*} Corresponding Author.

ambiguity) [19]. This often leads to logically contradictory comorbidities or clinically implausible comorbidity predictions. **Challenge 3: Absence of closed-loop self-correction.** Current unidirectional *input-to-output* workflows lack feedback mechanisms. When faced with ambiguous or conflicting candidates, these systems cannot re-examine original records for differential features, limiting accuracy in complex diagnostic scenarios.

Motivated by the above challenges, we propose RE-MCDF (Relation-Enhanced Multi-Expert Clinical Diagnosis Framework), entailing the following contributions:

- We establish a *generation-verification-revision* mechanism that integrates *primary*, *laboratory*, and *multi-relation group experts*. This iterative loop refines diagnoses through continuous feedback, emulating the rigorous traceability of real-world clinical consultations.
- To address heterogeneous and noisy EMR, we introduce a *laboratory expert* that dynamically prioritizes abnormal findings. This is coupled with a *KG-driven strategy* to balance diagnostic coverage for long-tail diseases with clinical specificity.
- We devise a multi-perspective evaluation mechanism where experts explicitly model *disease logic integration* and *clinical confusion* relationships. Furthermore, a novel relation-sensitive adjustment strategy with *bounded penalty* is applied, which strictly enforces logical consistency by penalizing conflicting candidates without artificially inflating unsupported diagnoses.
- Extensive experiments on the cerebrovascular disease subset of CMEMR (NEEMRs) and our own curated diagnostic corpus demonstrate (XMEMRs) that RE-MCDF outperforms state-of-the-art methods, validating the efficacy of our architectural design.

II. RELATED WORK

A. Disease Prediction from EMRs

Early EMR-based disease prediction primarily employed structured statistical or machine learning models that leverage tabular data (e.g., demographics, laboratory results, and diagnosis codes) [20], [21]. To address data complexity, subsequent work introduced multimodal fusion architectures [22] and privacy-preserving federated learning frameworks tailored for heterogeneous, multi-center EMRs [23]. More recently, LLMs have demonstrated strong capabilities in extracting insights from unstructured clinical narratives, achieving notable performance in mortality risk stratification [24], automated questionnaire generation [25], mental health concept classification [26], and adverse drug reaction identification [27]. Despite these advances, LLM-based approaches often yield *black-box* predictions that lack transparent, evidence-grounded reasoning chains. Moreover, they remain vulnerable to the high heterogeneity, sparsity, and intricate logical relationships among diseases, especially in complex domains like neurology [28], [29]. Consequently, existing methods fail to replicate the collaborative, relation-aware reasoning inherent in expert

diagnosis. To bridge this gap, we propose a *relation-enhanced multi-expert framework* that explicitly models inter-disease constraints and *enforces verifiable, closed-loop reasoning*.

B. KG-Enhanced Reasoning with LLMs

To enhance factual grounding and mitigate model hallucination, recent efforts integrate KGs into LLM-based reasoning. Early single-agent approaches inject external knowledge via KG-augmented prompting [13], in-context knowledge seeds [30], retrieval-augmented generation [31], [32], or iterative graph traversal [33], [34], and [35] further incorporates KG-constrained differential diagnosis with information-guided inquiry. While these methods improve accuracy, they place the full burden of evidence synthesis, logical inference, and error correction on a single agent, leading to error accumulation and limited reasoning depth. To distribute cognitive load, multi-agent frameworks have been proposed, where specialized agents collaborate on diagnosis [36]. For instance, [37] uses multi-agent debate to refine graph weights, while [38] employs linkage, retrieval, and prediction agents for zero-shot diagnosis. Some even leverage multi-LLM consensus for KG construction and validation [39]. However, most systems treat diseases as atomic labels rather than nodes in a relational network, focusing on surface-level agreement while neglecting disease-specific logical constraints (e.g., mutual exclusion). RE-MCDF addresses this by embedding relation-aware logic into a closed-loop framework, ensuring diagnostic conclusions are both knowledge-grounded and logically consistent.

III. PROPOSED METHOD

A. Problem Formulation

We consider a set of EMRs, each represented as $\mathbf{x} = \{x_{cc}, x_{hpi}, x_{pmh}, x_{pe}, x_{ae}\}$, which comprises the *chief complaint*, *history of present illness*, *past medical history*, *physical examination*, and *auxiliary examination*. By emulating the workflow of neurological expert consultations, we construct a multi-expert diagnostic network composed of a *primary expert* (\mathcal{A}_{pri}), a *laboratory expert* (\mathcal{A}_{lab}), and a *multi-relation awareness and evaluation group* (\mathcal{A}_{multi}). Additionally, we leverage a medical knowledge graph (MKG) $\mathcal{G} = (\mathcal{V}, \mathcal{M})$ as a structured knowledge substrate, where \mathcal{V} and \mathcal{M} denote the set of nodes (e.g., diseases, symptoms, and examinations) and the semantic relations connecting them. The objective is to generate a Top- k diagnostic set $\mathcal{D}_k = \{d_1, \dots, d_k\}$. To this end, as illustrated in Fig. 1, RE-MCDF establishes a *closed-loop diagnostic process*:

$$\mathcal{D}_k = \mathcal{F}_{\text{fusion}}(\mathcal{A}_{pri}, \mathcal{A}_{lab}, \mathcal{A}_{multi} \mid \mathbf{x}, \mathcal{G}) \xrightarrow{\text{feedback}} \mathcal{A}_{pri}, \quad (1)$$

where \mathcal{A}_{pri} generates initial diagnostic hypotheses and evidence pairs, \mathcal{A}_{lab} identifies abnormal indicators and computes dynamic weights for these entities, which are mapped to corresponding nodes in \mathcal{V} , and \mathcal{A}_{multi} analyzes inter-disease relationships to determine the final diagnosis. Furthermore, in the event of diagnostic conflicts, a feedback mechanism is triggered, prompting \mathcal{A}_{pri} to re-examine the original EMR for differential evidence. This iterative refinement ensures that

each diagnostic decision is supported by traceable clinical evidence and explicit logical justification.

B. Primary Diagnosis and Evidence Enhancement

In clinical practice, physicians infer diagnoses by synthesizing latent and heterogeneous evidence from the patient's chief complaint, laboratory results, and medical history. However, the scenarios we confront are characterized by high evidence heterogeneity, which renders traditional schemes such as named entity recognition (NER) and relation extraction (RE) suboptimal. Consequently, we introduce \mathcal{A}_{pri} to facilitate the generation of traceable evidence chains for subsequent validation through structured reasoning. Specifically, \mathcal{A}_{pri} executes a constrained CoT reasoning process: given a summarized medical record $\mathbf{s} = \text{Summarize}(\mathbf{x})$, the model outputs structured diagnosis-evidence pairs: $\mathcal{K}_{\text{pri}} = \{(d_i, \mathcal{E}_i)\}_{i=1}^N$, $\mathcal{E}_i = \{e_{i1}, \dots, e_{im}\}$, where d_i denotes a candidate disease and \mathcal{E}_i represents its supporting evidence entity. Let $\mathcal{E} = \{\mathcal{E}_1, \dots, \mathcal{E}_N\}$. To resolve semantic ambiguity, \mathcal{E} are aligned to a standard medical comparison table \mathcal{U} , resulting in a standardized entity set $\mathcal{E}_{\text{std}} = \{e \mid \text{type}(e) \in \mathcal{T}\}$, where \mathcal{T} is a predefined set of functional categories, ensuring consistent semantic grounding and enables structured downstream reasoning.

Furthermore, in this scenario, the potential pathological evidence and its corresponding diagnostic weight vary substantially across individual cases; thus, a *one-size-fits-all* weighting scheme, prevalent in existing literature, often leads to erroneous judgments by neglecting case-specific critical indicators. To address this, we integrated NER with \mathcal{A}_{lab} to collaborate with downstream experts, which identifies abnormal indicators and assigns prioritized weights to pathological findings, thereby amplifying the influence of salient clinical evidence on downstream reasoning. Specifically, it first performs structural processing of the EMR via a medical NER model [40] to extract medical entities. Then, based on the patient's basic information summary \mathbf{s}_{base} and summary of inspection results \mathbf{s}_{exam} , \mathcal{A}_{lab} perform the following calculations:

$$\begin{cases} \mathbf{w} = \{w_{\text{type}(e)}\}_{\text{type}(e) \in \mathcal{T}} = \text{Norm}(\psi_{\text{wei}}(\mathbf{s}_{\text{base}}, \mathbf{s}_{\text{exam}}, \mathcal{E}_{\text{std}})), \\ \mathcal{E}_{\text{abn}} = \psi_{\text{abn}}(\mathbf{s}_{\text{base}}, \mathbf{s}_{\text{exam}}, \mathcal{E}_{\text{std}}), \end{cases} \quad (2)$$

where, for each entity $e \in \mathcal{E}$, $w_{\text{type}(e)}$ denotes its base weight, $\text{Norm}(\cdot)$ is a normalization operation, which ensures $\sum_{\text{type}(e) \in \mathcal{T}} w_{\text{type}(e)} = 1$, while ψ_{wei} and ψ_{abn} represent the LLM-implemented reasoning logic of \mathcal{A}_{lab} for weight generation \mathbf{w} and abnormality identification \mathcal{E}_{abn} , respectively.

Although LLM-based approaches utilizing existing information can cover a majority of diagnostic scenarios, intrinsic knowledge limitations, particularly in smaller-scale models, inevitably lead to the omission of diagnoses, resulting in insufficient coverage of long-tail diseases [41]–[43]. To mitigate this deficiency, we leverage the established efficacy of MKG to provide an external knowledge base that compensates for the LLM's inherent shortcomings. Therefore, in our methodology, we integrate a MKG to supplement diagnoses that may be

overlooked by the LLM through structured knowledge. First, for \mathcal{E}_{std} , the entity-disease association strength is defined as:

$$\Gamma(e, d) = \begin{cases} 1, & \text{if } \text{dist}_{\mathcal{G}}(e, d) \leq 3, \\ 0, & \text{otherwise,} \end{cases} \quad (3)$$

where $\text{dist}_{\mathcal{G}}(e, d)$ denotes the shortest path length between e and d in the MKG. Subsequently, we map the entity weights to prioritize abnormal evidence:

$$w'_e = \begin{cases} 1.5w_{\text{type}(e)}, & e \in \mathcal{E}_{\text{abn}}, \\ w_{\text{type}(e)}, & \text{otherwise.} \end{cases} \quad (4)$$

Then, we propose a disease scoring function that balances evidence coverage, specificity, and connectivity:

$$S(d) = \alpha_1 V(d) + \alpha_2 C(d), \quad \alpha_1 + \alpha_2 = 1, \quad (5)$$

where $V(d) = \sum_{e \in \mathcal{E}_{\text{con}}(d, n)} \frac{w'_e}{\text{dist}_{\mathcal{G}}(e, d) + \varepsilon} / \sum_{e \in \mathcal{E}_{\text{con}}(d, n)} w'_e$ represents the weighted connectivity strength derived from the shortest path, $\mathcal{E}_{\text{con}}(d) = \{e \in \mathcal{E}_{\text{std}} \mid 1 \leq \text{dist}_{\mathcal{G}}(e, d) \leq 3\}$, and $\varepsilon = 10^{-8}$ is a smoothing factor. Also, the weighted evidence coverage is defined as $C(d) = \sum_{e \in \mathcal{E}_{\text{std}}} w'_e \Gamma(e, d) / \sum_{e \in \mathcal{E}_{\text{std}}} w'_e$.

Finally, the $\text{Top-}\hat{k}_{\text{sup}}$ diseases ranked by $S(d)$ are selected to form the supplementary candidate set \mathcal{D}_{sup} .

C. Multi-Expert Collaborative Evaluation

As discussed above, although initial disease-evidence pairs can be generated by a single agent, such models struggle to reason over complex inter-disease dependencies, including mutual exclusivity, comorbidity versus causality, and diagnostic confusion. To overcome these limitations, recent work has explored collaborative reasoning paradigms that combine multiple independent perspectives with external evidence constraints [44]–[46]. Building upon this, we introduce $\mathcal{A}_{\text{multi}}$, consisting of four specialized agents: *single-disease assessment expert* (\mathcal{A}_{sin}), *disease logic integration expert* (\mathcal{A}_{exc}), *confusion expert* ($\mathcal{A}_{\text{conf}}$), and *adjustment expert* (\mathcal{A}_{adj}).

1) *Single-Disease Evidence Expert*: As the foundational stage of the multi-expert collaborative evaluation, \mathcal{A}_{sin} assesses the plausibility of the initial diagnostic evidence and the alignment between candidate diseases and the critical indicators identified by \mathcal{A}_{lab} . Specifically, \mathcal{A}_{sin} utilizes structural grounding from \mathcal{G} to quantify the degree of match between a disease and the patient's clinical presentation, which processes three core categories of input: (i) the set of candidate diseases $\mathcal{D}_{\text{cand}}$ derived from \mathcal{K}_{pri} and \mathcal{D}_{sup} , (ii) \mathcal{E}_{abn} identified by \mathcal{A}_{lab} , and (iii) the disease-evidence connectivity paths derived from \mathcal{G} . The evidence consistency score is defined as:

$$\mathcal{F}_{\text{evid}}(d) = \mathcal{A}_{\text{sin}}(\mathcal{C}_{\mathcal{G}}(d), \mathcal{E}_{\text{abn}}, \mathbf{s}), \quad (6)$$

where $\mathcal{A}_{\text{sin}}(\cdot)$ is a output based on existing input of \mathcal{A}_{sin} , and $\mathcal{C}_{\mathcal{G}}(d) = \mathcal{N}_{\text{dir}}(d) \cup \mathcal{N}_{\text{path}}(d, \mathcal{E}_{\text{std}})$ provides the structured knowledge context for disease d . Here, $\mathcal{N}_{\text{dir}}(d) = \{(d, r_i, t_i) \in \mathcal{G}\}$ represents the set of triples directly incident to d , where r_i denotes the medical relation (e.g., *has_symptom* or *belongs_to*)

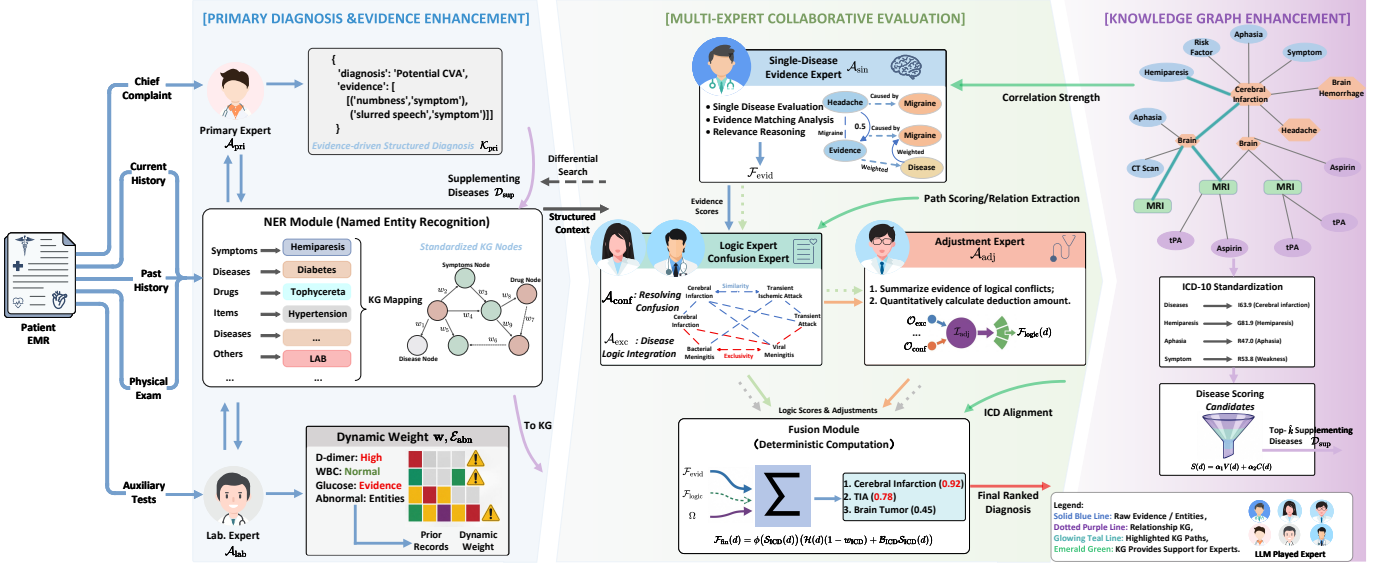


Fig. 1: Architecture of RE-MCDF. Consists of a primary expert that generates initial diagnosis–evidence pairs from EMRs, and a laboratory expert that dynamically weights heterogeneous clinical indicators (e.g., abnormal laboratory findings). A MKG is then used to expand candidate coverage and provide structured relational paths to four collaborative experts: single-disease assessment, disease logic integration, confusion detection, and logical adjustment. Together, these experts enforce logical consistency through relation-aware scoring and trigger closed-loop feedback when conflicts are detected (e.g., mutually exclusive diseases with similar confidence), enabling traceable and clinically plausible diagnostic reasoning.

and t_i is the corresponding target entity (e.g., a specific symptom or disease category). Meanwhile, $\mathcal{N}_{\text{path}}(d, \mathcal{E}_{\text{std}})$ encompasses all triples situated along the shortest paths from evidence entities $e_j \in \mathcal{E}_{\text{std}}$ to the candidate disease d . The scoring process explicitly emphasizes two factors:

- **Path Semantic Quality:** A weight-decay mechanism is applied based on path directness: direct relations (e.g., “Hypertension $\xrightarrow{\text{presentation}}$ High Blood Pressure”) receive higher weights, while indirect multi-hop paths (e.g., “Chronic Hypertension $\xrightarrow{\text{causes}}$ Cerebral Arteriolar Hyalinosis $\xrightarrow{\text{results in}}$ Deep White Matter Lacunar Infarction”) are progressively attenuated.
- **Priority of Abnormal Entities:** \mathcal{E}_{abn} is introduced (see (4)), ensuring that clinically critical findings exert greater influence on the final score.

2) *Multi-Disease Relation Awareness:* To better capture inter-disease dynamics (e.g., mutual exclusion, coexistence, causality, and differential ambiguity), we design \mathcal{A}_{exc} and $\mathcal{A}_{\text{conf}}$, which reason over relational structures extracted from \mathcal{G} , based on two specialized relationship sets: the *pathological compatibility relationship* \mathcal{R}_{exc} and the *clinical confusion relationship* $\mathcal{R}_{\text{conf}}$. Notably, they produce a *logical confidence score* $\mathcal{F}_{\text{logic}}(d)$ of candidate diseases, which serves as the primary metric for finalizing the diagnostic set \mathcal{D}_k .

To operationalize the logical constraints within \mathcal{A}_{exc} , we align the clinical diagnostic process with the fundamental principles of *collective exhaustivity* and *mutual exclusivity*. Specifically, guided by the taxonomic hierarchy of [19], we focus on the *pathological compatibility* within the initial

candidate set. Unlike generalized semantic similarity, this relationship characterizes the *biological compatibility* between entities, a critical mechanism for pruning logically implausible disease combinations. These constraints are explicitly derived from the *pathological subtype edges* in \mathcal{G} , formalized as: $\mathcal{R}_{\text{exc}} = \{(d_i, d_j, e) \mid \hat{r}(d_i, d_j) \in \mathcal{G}, q \in \mathcal{P}_{\text{str}}\}$, where \hat{r} denotes predefined pathological typing relations, \mathcal{P}_{str} denotes the set of structured evidence paths, and q is a path indicating pathological exclusivity (e.g., “HER2 Positive $\xleftarrow{[\text{Type}]}$ HER2 Negative”). This formulation captures three types of strict exclusivity: (i) Mutually exclusive molecular subtypes of the same disease (e.g., EGFR-mutant vs. ALK-rearranged); (ii) Mutually exclusive pathological classification standards (e.g., Type 1 vs. Type 2 Diabetes); (iii) Chronologically distinct disease stages (e.g., Acute vs. Old Myocardial Infarction). Accordingly, \mathcal{A}_{exc} reasons on the structured input \mathcal{C}_{exc} based on the predefined output conditions \mathcal{P}_{exc} , yielding \mathcal{O}_{exc} :

$$\begin{cases} \mathcal{C}_{\text{exc}} = \bigcup_{(d_i, d_j) \in \mathcal{R}_{\text{exc}}} \{\text{evid}_{\text{path}}(d_i, d_j)\} \cup \{\mathcal{C}_{\text{pt}}, \mathcal{D}_{\text{cand}}\}, \\ \mathcal{O}_{\text{exc}} = \mathcal{A}_{\text{exc}}(\mathcal{C}_{\text{exc}}, \mathcal{P}_{\text{exc}}), \end{cases} \quad (7)$$

where \mathcal{C}_{pt} represents the patient context, $\text{evid}_{\text{path}}(d_i, d_j)$ denotes the MKG path substantiating exclusivity between d_i and d_j , and $\mathcal{A}_{\text{exc}}(\cdot)$ is the output of \mathcal{A}_{exc} . While, the implementation of clinical confusion relations is more challenging, as relying solely on MKG is insufficient for comprehensive coverage. Therefore, we design a dual confusion discrimination mechanism for $\mathcal{A}_{\text{conf}}$: (i) Explicit differential diagnosis edges \bar{r} in MKG; (ii) Attribute overlap analysis based on core

clinical features (symptoms/imaging/biochemistry), defined as: $\mathcal{R}_{\text{conf}} = \{(d_i, d_j) \mid \bar{r}(d_i, d_j) \in \mathcal{G} \vee |\xi(d_i, d_j)| \geq 2\}$, where $\xi(d_i, d_j) = \Phi(d_i) \cap \Phi(d_j)$ represents the *feature overlap set*, characterizing the diagnostic intersection between two candidate diseases, and $\Phi(d)$ denotes the set of core clinical features associated with disease d . Consequently, the input evidence structure $\mathcal{C}_{\text{conf}}$ and the verified output $\mathcal{O}_{\text{conf}}$ of $\mathcal{A}_{\text{conf}}$ are defined as:

$$\begin{cases} \mathcal{C}_{\text{conf}} = \bigcup_{(d_i, d_j) \in \mathcal{R}_{\text{conf}}} \left\{ \begin{array}{l} \mathcal{I}_{\text{share}} = \xi_{\text{type}(e)}(d_i, d_j), \\ \mathcal{I}_{\text{diff}} = \Phi(d_i) \Delta \Phi(d_j), \\ \mathcal{I}_{\mathcal{G}} = \text{path}_{\mathcal{G}}(d_i, d_j), \end{array} \right\} \cup \mathcal{C}_{\text{pt}}, \\ \mathcal{O}_{\text{conf}} = \mathcal{A}_{\text{conf}}(\mathcal{C}_{\text{conf}}, \mathcal{P}_{\text{conf}}), \end{cases} \quad (8)$$

where $\mathcal{A}_{\text{conf}}(\cdot)$ is the output of $\mathcal{A}_{\text{conf}}$, $\mathcal{I}_{\text{share}}$ represents the evidence derived from shared features, $\mathcal{I}_{\text{diff}}$ denotes the *discriminative attributes* calculated via the symmetric difference Δ , $\mathcal{I}_{\mathcal{G}}$ denotes explicit associative paths in \mathcal{G} , and the expert assessment protocol $\mathcal{P}_{\text{conf}}$ enforces a rigorous *logical verification* mechanism. Then, the relational sets \mathcal{O}_{exc} and $\mathcal{O}_{\text{conf}}$ are aggregated into a comprehensive context \mathcal{I}_{adj} , which serves as the input set for \mathcal{A}_{adj} :

$$\mathcal{I}_{\text{adj}} = \mathcal{D}_{\text{cand}} \cup \mathcal{O}_{\text{exc}} \cup \mathcal{O}_{\text{conf}} \cup \mathcal{C}_{\text{pt}}. \quad (9)$$

To ensure clinical robustness, \mathcal{A}_{adj} processes this context to generate the logical confidence score $\mathcal{F}_{\text{logic}}(d)$, subject to three strict properties:

- *Bounded Penalty*: $\mathcal{F}_{\text{logic}}(d) \in [0, 1]$, preventing evidence-free inflation.
- *Relation-Sensitive Attenuation*: (i) For \mathcal{O}_{exc} , weaker candidates incur stronger penalties ($\mathcal{F}_{\text{logic}} \rightarrow 0$). (ii) For $\mathcal{O}_{\text{conf}}$, all relevant candidates are synchronously attenuated based on clinical feature uncertainty.
- *Default Consistency*: For candidates not involved in verification relations, the system maintains original confidence by setting $\mathcal{F}_{\text{logic}}(d) = 1$.

Finally, guided by the aforementioned constraints and inputs, \mathcal{A}_{adj} execute clinical logical reasoning, with the output strictly constrained to a *piecewise structure*:

$$\mathcal{F}_{\text{logic}}(d) = \begin{cases} \mathcal{A}_{\text{adj}}(d, \mathcal{I}_{\text{adj}}), & \text{if } d \in \text{Dom}(\mathcal{O}_{\text{exc}} \cup \mathcal{O}_{\text{conf}}), \\ 1, & \text{otherwise,} \end{cases} \quad (10)$$

where $\text{Dom}(\cdot)$ denotes the *domain of influence* (i.e., the set of disease entities involved in identified logical relationships), and $\mathcal{A}_{\text{adj}}(\cdot)$ is the output of \mathcal{A}_{adj} .

3) *Final diagnosis generation*: We implement a *multi-tiered fusion strategy* to compute the finalized scores for candidate diseases. We first calculates a *core composite score* $\mathcal{H}(d) = \beta_1 \mathcal{F}_{\text{evid}}(d) + \beta_2 \mathcal{F}_{\text{logic}}(d) + \beta_3 \Omega(d)$, where $\Omega(d)$ denotes the graph connectivity score between the disease and evidence entities, $\sum_{i=1}^3 \beta_i = 1$, and then incorporates an *ICD-10 standardization penalty mechanism* [19] to generate a diagnostic ranking that aligns with clinical practice:

$$\mathcal{F}_{\text{fin}}(d) = \phi(\mathcal{S}_{\text{ICD}}(d))(\mathcal{H}(d)(1 - w_{\text{ICD}}) + \mathcal{B}_{\text{ICD}}\mathcal{S}_{\text{ICD}}(d)), \quad (11)$$

TABLE I: Statistical comparison of datasets. Average input length aggregates all structured clinical fields (e.g., history, examinations, and results).

Dataset	Samples	Avg. Labels	Avg. Len.
NEEMRs (Public)	1,001	2.75	582.4
XMEMRs (Self-constructed)	1,024	5.48	2,779.2

where $\mathcal{S}_{\text{ICD}}(d)$ represents the normalized ICD-10 standardization similarity score, \mathcal{B}_{ICD} serves as the weight for ICD-related features and w_{ICD} controls the contribution of the ICD alignment term. Also, the *penalty function* $\phi(\cdot)$ is defined as:

$$\phi(\mathcal{S}_{\text{ICD}}(d)) = \begin{cases} 1, & \text{if } \mathcal{S}_{\text{ICD}}(d) \geq \tau_{\text{thr}}, \\ \left(\frac{\mathcal{S}_{\text{ICD}}(d)}{\tau_{\text{thr}}}\right)^{\gamma}, & \text{otherwise,} \end{cases} \quad (12)$$

where τ_{thr} is the predefined ICD compliance threshold and γ denotes the penalty intensity coefficient. Finally, diseases are ranked by \mathcal{F}_{fin} , and the Top- k are returned as \mathcal{D}_k .

IV. EXPERIMENTS AND EVALUATIONS

In this section, we first detail the datasets and experimental settings. Subsequently, we present a comparative analysis between RE-MCDF and representative methods. Finally, we conduct ablation studies to verify the effectiveness of the specific modules within RE-MCDF.

A. Datasets

To evaluate the performance of RE-MCDF across both standardized benchmarks and real-world clinical scenarios, we conducted experiments on two distinct datasets.

NEEMRs (Public Benchmark): We utilize the neurology subset of the CMEMR [11], where each record contains core clinical fields including the chief complaint, basic information, history of present illness (HPI), past medical history (PMH), physical examination, and auxiliary examination.

XMEMRs (Self-constructed Clinical Dataset): Due to the scarcity of high-quality neurology EMR datasets in existing research, we constructed XMEMRs, a neurology-focused EMR dataset designed to reflect high-complexity real-world clinical scenarios. The dataset was collected from the Department of Neurology at a Grade-A Tertiary Hospital between 2024 and 2025. All records underwent rigorous quality control by three senior neurologists, who excluded cases with missing information, inconsistent documentation, or insufficient diagnostic evidence. The remaining records were then standardized and manually annotated with confirmed diagnoses. Compared to NEEMRs, XMEMRs contains more comprehensive primary examination data, including sequential laboratory results, imaging reports, and electrocardiograms (ECGs), making it more challenging and clinically realistic. A statistical comparison between the two datasets is provided in Table I.

B. Implementation Details

Medical Knowledge Graph: We utilize CPubMed-KGv2 (1.7 million nodes, 3.9 million relations). Shortest path calculations

TABLE II: Experimental results on NEEMRs and XMEMRs datasets across different LLM backbones. All metrics are reported in percentage (%), where **R**, **P** and **F1** stands for Recall, Precision, and F1 Score.

Methods	Qwen2.5-7B-Instruct						GLM-4-9B						
	NEEMRs			XMEMRs			NEEMRs			XMEMRs			
	R	P	F1	R	P	F1	R	P	F1	R	P	F1	
<i>LLM-only</i>	CoT [4]	37.80	39.03	38.40	35.01	32.85	33.90	41.29	39.50	40.37	37.33	35.80	36.55
	ToT [5]	42.23	38.68	40.38	33.71	31.01	32.30	39.94	36.71	38.26	38.82	35.62	37.15
	Sc-CoT [6]	44.23	30.44	36.06	31.03	34.62	32.73	39.58	35.19	37.25	38.10	35.00	36.48
<i>LLM⊕KG</i>	MindMap [13]	45.54	41.91	43.65	38.46	36.45	37.43	43.54	40.22	41.82	35.48	38.40	36.88
	ICP [30]	40.96	37.87	39.36	34.01	32.50	33.24	37.25	36.78	37.01	38.10	34.86	36.41
	KG-Rank [32]	38.34	35.22	36.71	35.39	32.42	33.83	40.00	33.33	36.36	34.19	37.38	35.72
<i>LLM⊗KG</i>	MedIKAL [11]	41.32	41.63	41.47	38.24	38.32	38.28	40.71	39.45	40.07	38.77	37.91	38.34
	Graph-CoT [34]	45.43	41.66	43.46	40.64	37.06	38.76	42.07	38.78	40.36	38.45	37.87	38.16
<i>Multi-Agent</i>	MAGIC [37]	35.61	33.32	34.42	34.88	33.26	34.05	36.67	36.67	36.67	38.30	35.17	36.67
	KERAP [38]	33.87	40.32	36.81	33.14	37.10	35.01	36.25	38.78	37.47	37.88	36.70	37.28
RE-MCDF (Ours)	46.13	42.28	44.11	42.33	38.78	40.48	44.20	40.47	42.25	42.23	38.69	40.38	

are accelerated via Neo4j GDS. For ICD-10 standardization, we follow [11], [47], adopting a fuzzy string matching algorithm with a similarity threshold set to 0.5.

Model Configuration: Qwen2.5-7B-Instruct and GLM-4-9B (bfloat16 precision) serves as the backbone model, loaded via vLLM with the temperature set to 0 to ensure deterministic outputs. For NER, we employ the medical-domain RaNER model [40] to identify 9 categories of entities (i.e., $\mathcal{T} = \{\text{sym}, \text{dis}, \text{dru}, \text{bod}, \text{ite}, \text{equ}, \text{mic}, \text{dep}, \text{pro}\}$), and we use Bge-small-zh for embeddings.

Baseline: We compared RE-MCDF with four series of baseline methods: LLM-only, LLM \oplus KG, LLM \otimes KG and multi-agent combination KG. **LLM-only**: They only use the LLMs’ internal knowledge for reasoning, including CoT [4], ToT [5] and Sc_Cot [6]. **LLM \oplus KG**: We selected there representative works, namely MindMap [13], ICP [30] and KG-Rank [32], all of which are aimed at medical question-answering and reasoning tasks. **LLM \otimes KG**: We select Medikal [11] and Graph-Cot [34]. **Multi-agent combination KG**: We implemented a multi-agent framework for the medical field combined with KG, which is of the same type as RE-MCDF, MAGIC [37], KERAP [38].

C. Performance Comparison with Baseline Methods

Table II compares RE-MCDF against the baselines across four technical categories. Overall, our framework consistently achieves state-of-the-art (SOTA) performance across all backbones. Compared to LLM-only approaches, RE-MCDF exhibits a substantial leap; on NEEMRs (Qwen2.5), it achieves an F1 of 44.11%, surpassing Sc-CoT and ToT by gains of 8.05% and 3.73%. This highlights the limitations of vanilla LLMs, where clinical noise often impedes reasoning without structured validation. Furthermore, RE-MCDF consistently outperforms knowledge-enhanced (e.g., MindMap), tightly-

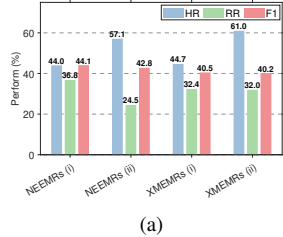
coupled (e.g., MedIKAL), and multi-agent (e.g., KERAP) systems. By explicitly modeling logical interdependencies, RE-MCDF effectively overcomes the knowledge noise and conflicting reasoning paths prevalent in these advanced architectures, ensuring more precise evidence alignment in complex diagnostic tasks. The superiority of RE-MCDF remains consistent when scaling to the GLM-4 backbone. In the more challenging XMEMRs scenario, RE-MCDF (F1 = 40.38%) significantly outperforms the strongest knowledge-enhanced baselines, such as MedIKAL (38.34%) and Graph-CoT (38.16%). Notably, while most baselines exhibit unstable cross-dataset performance, suffering significant drops on XMEMRs under Qwen2.5 or inconsistent fluctuations under GLM-4, RE-MCDF consistently achieves the highest F1 and superior robustness. On NEEMRs and XMEMRs, outperforming all competitors, thereby confirming its resilience in complex real-world diagnostics.

TABLE III: Ablation study results of the RE-MCDF on NEEMRs and XMEMRs (*Qwen2.5; all metrics in %*).

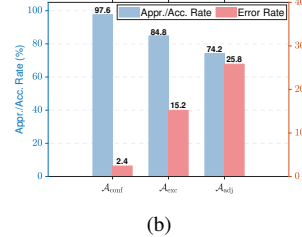
Config.	NEEMRs			XMEMRs		
	R	P	F1	R	P	F1
RE-MCDF	46.13	42.28	44.11	42.33	38.78	40.48
w/o \mathcal{G}_{MKG}	44.12	40.43	42.20	40.14	36.70	38.34
w/o \mathcal{A}_{lab}	43.50	40.46	41.70	39.49	36.11	37.73
w/o \mathcal{A}_{sin}	44.13	40.45	42.21	40.18	36.73	38.37
w/o \mathcal{A}_{rel}	45.72	41.90	43.72	40.27	36.94	38.54
LLM-direct	41.79	40.78	41.28	36.96	33.89	35.35

D. Ablation Study-I

As illustrated in Table III, the full RE-MCDF model consistently achieves the optimal performance across all datasets (in-



(a)



(b)

Fig. 2: Performance analysis and human evaluation. Left subplot: Impact of MKG supplement depth \hat{k}_{sup} on retrieval and verification ($\hat{k}_{\text{sup}} = 1$ for (i), $\hat{k}_{\text{sup}} = 2$ for (ii)). Right subplot: Manual evaluation of reasoning trajectories, where $\mathcal{A}_{\text{conf}}$ and \mathcal{A}_{exc} are measured by physician approval rate, and \mathcal{A}_{adj} by accuracy rate (Based on Qwen2.5).

cluding methods for directly predicting diseases using LLMs). Interestingly, \mathcal{A}_{lab} emerges as the most critical component for diagnostic accuracy; its removal leads to the most significant F1 drop of 2.41% and 2.75% on NEEMRs and XMEMRs. This highlights the importance of dynamic evidence weighting in clinical practice. The \mathcal{G}_{MKG} and \mathcal{A}_{sin} modules also play vital roles, particularly in ensuring diagnostic coverage for complex cases, with their absence resulting in F1 declines of 2.14% and 2.11% for XMEMRs, respectively. Furthermore, \mathcal{A}_{rel} (i.e., $\mathcal{A}_{\text{exc}} + \mathcal{A}_{\text{conf}}$) module ensures logical consistency by filtering out contradictory diagnoses (e.g., mutually exclusive stroke types). Disabling this module causes the F1 to fall to 38.54% on XMEMRs. Manual review confirms that \mathcal{A}_{rel} successfully resolved logical conflicts in 17.8% of analyzed cases, preventing common diagnostic pitfalls. These results demonstrate that the synergy between structured knowledge, expert-based evidence weighting, and logical relationship mining is essential for superior clinical decision support.

E. Ablation Study-II

To evaluate the effectiveness of the MKG supplement mechanism, we define two metrics: hit rate (HR), which measures initial coverage (i.e., whether one supplement matches ground truth via fuzzy matching), and retained-and-hit rate (RR), which measures the proportion of supplemented candidates that are successfully verified by \mathcal{A}_{sin} and \mathcal{A}_{rel} and retained in the final Top- \hat{k} . As shown in Fig. 2 (a), while HR increases monotonically with \hat{k}_{sup} , RR stagnates or even declines significantly. For the NEEMRs dataset, increasing \hat{k}_{sup} from 1 to 2 leads to a sharp 12.3% relative drop in RR (36.8% \rightarrow 24.5%). This phenomenon reveals an “attention dilution” effect: a single high-confidence supplement ($\hat{k}_{\text{sup}} = 1$) allows \mathcal{A}_{sin} , \mathcal{A}_{rel} to focus on precise evidence matching and logical verification. Conversely, higher \hat{k}_{sup} values introduce irrelevant candidates that act as noise, overwhelming the experts with complex relational paths and increasing the risk of false suppression of true diagnoses. This degradation is more pronounced on the NEEMRs dataset due to its lower diagnostic density (2.75 labels/case vs. 5.48 in XMEMRs). In such sparse scenarios, extra candidates are more likely to lack clinical relevance, misallocating the multi-expert system’s computational focus

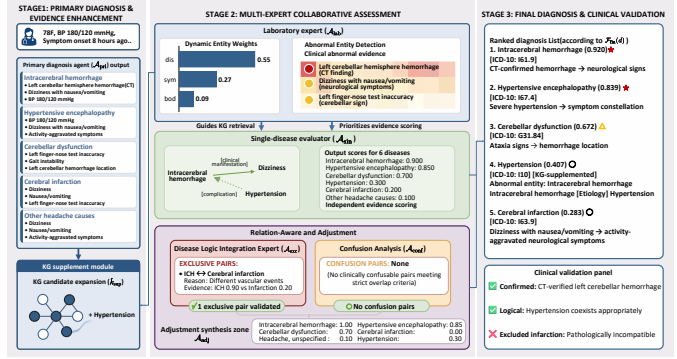


Fig. 3: Illustrative case study of RE-MCDF: Integrating clinical evidence with relation-aware reasoning.

and hindering the retention of correct diagnoses. Across both datasets, $\hat{k}_{\text{sup}} = 1$ yields the optimal F1, validating our *precision over breadth* design principle. This aligns with clinical heuristics where experienced physicians prioritize 1–2 key differential diagnoses for in-depth verification.

F. Ablation Study-III

1) *Fine grained analysis of expert collaboration mechanism:* To verify clinical reliability, senior neurologists conducted a blind review of reasoning trajectories sampled from XMEMRs, focusing on logical consistency and weighting rationality. As shown in Fig. 2 (b), \mathcal{A}_{exc} achieved an 84.8% approval rate (39/46), correctly modeling pathological relationships such as mutual exclusivity (e.g., hemorrhage vs. infarction), coexistence, and causality (e.g., atrial fibrillation leading to stroke). The remaining 15.2% of errors were primarily attributable to oversimplified modeling of complex complications. $\mathcal{A}_{\text{conf}}$ demonstrated exceptional utility with a 97.6% (362/371) success rate in identifying critical differential pairs, such as distinguishing BPPV from Meniere’s disease based on positional triggers. Only 2.4% were mislabeled. Furthermore, \mathcal{A}_{adj} achieved 74.2% (144/194) accuracy in executing logical weight modifications. These results confirm that RE-MCDF’s gains stem from rigorous clinical reasoning rather than simple probabilistic pattern matching.

2) *Qualitative analysis of cases:* Fig. 3 illustrates RE-MCDF’s diagnostic trajectory for a 78-year-old female with acute vertigo and CT-confirmed cerebellar hemorrhage. This case highlights three key strengths of the framework: (i) *Priority Weighting:* \mathcal{A}_{lab} assigns a high weight (0.55) to the critical indicator *cerebellar hemorrhage*, preventing diagnostic drift toward nonspecific symptoms such as nausea or dizziness; (ii) *Logic Enforcement:* \mathcal{A}_{exc} identifies the *mutual exclusivity* between hemorrhage and infarction; accordingly, \mathcal{A}_{adj} assigns a 0.0 compatibility score, effectively eliminating symptom-driven misdiagnoses (e.g., nausea); (iii) *MKG Augmentation:* The supplement module identifies hypertension (4th, score 0.407), matching the ground truth *hypertension grade 3*. The final ranking (cerebral hemorrhage 0.920 $>$ hypertensive encephalopathy 0.839 $>$ hypertension 0.407) perfectly aligns

with the clinical hierarchy, with the acute event as the primary diagnosis and hypertension as the etiological factor.

V. CONCLUSION AND FUTURE WORK

In this paper, we presented RE-MCDF, a relation-enhanced multi-expert framework that addresses evidence heterogeneity and logical inconsistencies in EMR reasoning. By introducing a *generate-verify-revise closed-loop* mechanism, RE-MCDF emulates the deliberative and collaborative workflow of real-world clinical consultations. Experimental results on the NEEMRs and XMEMRs datasets demonstrate that RE-MCDF outperforms the existing baselines. Three avenues of research constitute promising future directions: (i) Integrating medical imaging (e.g., CT/MRI) with textual EMRs to enhance diagnostic depth; (ii) Validating the framework's efficacy across other complex medical specialties beyond neurology; (iii) Optimizing reasoning efficiency for real-time integration into hospital decision support systems.

REFERENCES

- [1] J. Mayourian, W. G. La Cava *et al.*, “Expert-Level Automated Diagnosis of the Pediatric ECG Using a Deep Neural Network,” *JACC Clin. Electrophysiol.*, vol. 11, no. 6, pp. 1308–1320, 2025.
- [2] X. Dong, K. Yang *et al.*, “Cross-Domain Mutual-Assistance Learning Framework for Fully Automated Diagnosis of Primary Tumor in Nasopharyngeal Carcinoma,” *IEEE Trans. Med. Imag.*, vol. 43, no. 11, pp. 3676–3689, 2024.
- [3] S. Zhou, Z. Xu *et al.*, “Large Language Models for Disease Diagnosis: A Scoping Review,” *NPJ Artif. Intell.*, vol. 1, no. 9, pp. 1–17, 2025.
- [4] J. Wei *et al.*, “Chain-of-Thought Prompting Elicits Reasoning in Large Language Models,” in *NeurIPS*, vol. 35, 2022, pp. 24 824–24 837.
- [5] S. Yao, D. Yu *et al.*, “Tree of Thoughts: Deliberate Problem Solving with Large Language Models,” in *NeurIPS*, vol. 36, 2023, pp. 11 809–11 822.
- [6] X. Wang, J. Wei *et al.*, “Self-Consistency Improves Chain of Thought Reasoning in Language Models,” in *ICLR*, 2023.
- [7] S. Li, C. Zheng *et al.*, “Verification is All You Need: Prompting Large Language Models for Zero-Shot Clinical Coding,” *IEEE J. Biomed. Health Inform.*, vol. 29, no. 11, pp. 8536–8549, 2025.
- [8] Y. Wu, G. Wan *et al.*, “Mind AI’s Mind: A Clinically Aligned Explainable AI Pipeline for Depression Diagnosis via Large Language Models,” *IEEE Trans. Affect. Comput.*, pp. 1–1, 2025.
- [9] Y. Gao, R. Li *et al.*, “Leveraging Medical Knowledge Graphs Into Large Language Models for Diagnosis Prediction: Design and Application Study,” *JMIR AI*, vol. 4, 2025.
- [10] Y. Liu, S. Li *et al.*, “CoG: Controllable Graph Reasoning via Relational Blueprints and Failure-Aware Refinement over Knowledge Graphs,” *arXiv preprint arXiv:2601.11047*, 2026.
- [11] M. Jia, J. Duan *et al.*, “MedIKAL: Integrating Knowledge Graphs as Assistants of LLMs for Enhanced Clinical Diagnosis on EMRs,” in *COLING*, 2025, pp. 9278–9298.
- [12] J. Mandravickaitė, “Narrative Structure Extraction in Disinformation and Trustworthy News: A Comparison of LLM, KG, and KG-Augmented Pipelines,” in *Workshops of KONVENS*, 2025, pp. 86–103.
- [13] Y. Wen, Z. Wang *et al.*, “MindMap: Knowledge Graph Prompting Sparks Graph of Thoughts in Large Language Models,” in *ACL*, 2024, pp. 10 370–10 388.
- [14] J. Jiang, K. Zhou *et al.*, “KG-Agent: An Efficient Autonomous Agent Framework for Complex Reasoning over Knowledge Graph,” in *ACL*, 2025, pp. 9505–9523.
- [15] S. Singh *et al.*, “AdaptBot: Combining LLM with Knowledge Graphs and Human Input for Generic-to-Specific Task Decomposition and Knowledge Refinement,” in *ICRA*, 2025, pp. 4345–4351.
- [16] H. Li, X. Cheng *et al.*, “Accurate Insights, Trustworthy Interactions: Designing a Collaborative AI-Human Multi-Agent System with Knowledge Graph for Diagnosis Prediction,” in *CHI*, 2025.
- [17] X. Li, Wanghaijiao *et al.*, “Knowledge-Aware Co-Reasoning for Multi-disciplinary Collaboration,” in *EMNLP*, 2025, pp. 13 604–13 620.
- [18] D. H. Ho, U. Das *et al.*, “Leveraging Multi-Agent Systems and Large Language Models for Diabetes Knowledge Graphs,” in *BigData*, 2024, pp. 3401–3410.
- [19] J. Zhou and A. Liu, “High-quality Disease Classification in Line with International Standards: Current Status and Reflections,” *Med. J. Peking Union Med. Coll. Hosp.*, vol. 15, no. 5, pp. 993–998, 2024.
- [20] N. Aminnejad, M. Greiver *et al.*, “Predicting the onset of chronic kidney disease (CKD) for diabetic patients with aggregated longitudinal EMR data,” *PLOS Digital Health*, vol. 4, no. 1, p. e0000700, 2025.
- [21] U. K. Mukherjee, H. Ye *et al.*, “Encounter Decisions for Patients With Diverse Sociodemographic Characteristics: Predictive Analytics of EMR Data From a Large Chain of Clinic,” *JOM*, 2025.
- [22] A. Al-Dailami, H. Kuang *et al.*, “Multimodal Representation Learning Based on Personalized Graph-Based Fusion for Mortality Prediction Using Electronic Medical Records,” *Big Data Min. Anal.*, vol. 8, no. 4, pp. 933–950, 2025.
- [23] A. Al-Dailami *et al.*, “FedComDist: Towards Effective Personalized Federated Learning for Patient Outcome Prediction Using Multi-Center Electronic Medical Records,” *IEEE J. Biomed. Health*, vol. 29, no. 8, pp. 6004–6016, 2025.
- [24] D. Anderson, M. Anderson *et al.*, “Paging Dr. GPT: Extracting Information from Clinical Notes to Enhance Patient Predictions,” *arXiv preprint arXiv:2504.12338*, 2025.
- [25] R. Ding, Q. Sun *et al.*, “From EMR Data to Clinical Insight: An LLM-Driven Framework for Automated Pre-Consultation Questionnaire Generation,” *arXiv preprint arXiv:2508.00581*, 2025.
- [26] N. C. Cardamone, M. Olfson *et al.*, “Classifying unstructured text in electronic health records for mental health prediction models: large language model evaluation study,” *JMIR Med. Inf.*, vol. 13, no. 1, p. e65454, 2025.
- [27] Y. L. Koon, H. X. Tan *et al.*, “Unlocking potential of generative large language models for adverse drug reaction relation prediction in discharge summaries: analysis and strategy,” *Clin. Pharmacol. Ther.*, vol. 118, no. 6, pp. 1554–1561, 2025.
- [28] Y. Kang, M. Yang *et al.*, “LLM-DG: Leveraging large language model for enhanced disease prediction via inter-patient and intra-patient modeling,” *Inform. Fusion*, vol. 121, p. 103145, 2025.
- [29] H. Lu and U. Naseem, “Can Large Language Models Enhance Predictions of Disease Progression? Investigating Through Disease Network Link Prediction,” in *EMNLP*, 2024.
- [30] J. Wu, X. Wu *et al.*, “Guiding Clinical Reasoning with Large Language Models via Knowledge Seeds,” in *IJCAI*, 2024, pp. 7491–7499.
- [31] X. Jiang, R. Zhang *et al.*, “HyKGE: A Hypothesis Knowledge Graph Enhanced RAG Framework for Accurate and Reliable Medical LLMs Responses,” in *ACL*, 2025, pp. 11 836–11 856.
- [32] R. Yang, H. Liu *et al.*, “KG-Rank: Enhancing Large Language Models for Medical QA with Knowledge Graphs and Ranking Techniques,” in *Workshop on BNLP*, 2024, pp. 155–166.
- [33] J. Sun, C. Xu *et al.*, “Think-on-Graph: Deep and Responsible Reasoning of Large Language Model on Knowledge Graph,” in *ICRL*, vol. 2024, 2024, pp. 3868–3898.
- [34] B. Jin, C. Xie *et al.*, “Graph Chain-of-Thought: Augmenting Large Language Models by Reasoning on Graphs,” in *Findings of ACL*, 2024, pp. 163–184.
- [35] Q. Wang, R. Sheng *et al.*, “MedKGI: Iterative Differential Diagnosis with Medical Knowledge Graphs and Information-Guided Inquiring,” *arXiv preprint arXiv:2512.24181*, 2025.
- [36] J. Sun, C. Xu *et al.*, “MedLA: A Logic-Driven Multi-Agent Framework for Complex Medical Reasoning with Large Language Models,” in *AAAI*, 2026, pp. 1–1.
- [37] B. Liu, Y. Nie *et al.*, “MAGIC: AN LLM-based Multi-agent Activated Graph-reasoning Intelligent Collaboration model for Liver Disease Diagnosis,” *Inform. Fusion*, vol. 126, p. 103557, 2026.
- [38] Y. Xie, H. Cui *et al.*, “KERAP: A Knowledge-Enhanced Reasoning Approach for Accurate Zero-shot Diagnosis Prediction Using Multi-agent LLMs,” in *AMIA*, 2025, pp. 1–1.
- [39] U. Das, K. B. Atmakuri *et al.*, “Clinical Knowledge Graph Construction and Evaluation with Multi-LLMs via Retrieval-Augmented Generation,” *arXiv preprint arXiv:2601.01844*, 2026.
- [40] X. Wang, Y. Jiang *et al.*, “Improving Named Entity Recognition by External Context Retrieving and Cooperative Learning,” in *EMNLP*, 2021, pp. 1800–1812.

- [41] S. Yu, R. Bao *et al.*, “Dynamic Uncertainty Ranking: Enhancing Retrieval-Augmented In-Context Learning for Long-Tail Knowledge in LLMs,” in *NAACL*, 2025, pp. 8985–8997.
- [42] Z. Yi, J. Ouyang *et al.*, “A Survey on Recent Advances in LLM-Based Multi-turn Dialogue Systems,” *ACM Comput. Surv.*, vol. 58, no. 6, 2025.
- [43] Y. Wu *et al.*, “Contrastive Learning with large language models for medical code prediction,” *Expert Syst. Appl.*, vol. 277, p. 127241, 2025.
- [44] D. Wan, J. Chen *et al.*, “MAMM-Refine: A Recipe for Improving Faithfulness in Generation with Multi-Agent Collaboration,” in *NAACL*, 2025, pp. 9882–9901.
- [45] H. Shi, S. Ye *et al.*, “Muma-Tom: Multi-modal Multi-agent Theory of Mind,” in *AAAI*, vol. 39, no. 2, 2025, pp. 1510–1519.
- [46] A. Ghafarollahi and M. J. Buehler, “SciAgents: Automating Scientific Discovery through Bioinspired Multi-agent Intelligent Graph Reasoning,” *Advanced Materials*, vol. 37, no. 22, p. 2413523, 2025.
- [47] Z. Fan, J. Tang *et al.*, “AI Hospital: Interactive Evaluation and Collaboration of LLMs as Intern Doctors for Clinical Diagnosis,” *arXiv preprint arXiv:2402.09742*, 2024.